Mathematical modeling of detonation initiation via flow cumulation effects

Ilya Semenov[*,**], *Pavel Utkin*[*,**], *Ildar Akhmedyanov*[*]
[*]*Institute for Computer Aided Design Russian Academy of Sciences*
2nd Brestskaya 19/18, Moscow, 123056, Russia
[**]*Moscow Institute of Physics and Technology*
Instituskiy per. 9, Dolgoprudny, 141700, Russia

Abstract
The paper concerns two problems connected with the idea of gaseous detonation initiation via flow cumulation effects and relatively weak shock waves convergence. The first one is three-dimensional numerical investigation of shock-to-detonation transition in methane-air mixture in a tube with parabolic contraction, connecting section of narrow diameter and conical expansion. The second problem is numerical study of the start-up of the small-scaled hydrogen electrochemical pulse detonation engine model with the use of electrical discharge which causes the toroidal shock wave. The investigation is performed by means of numerical experiment with the use of modern high performance computing systems.

1. Introduction

Theoretical studies of gaseous detonation initiation via flow cumulation effects and relatively weak shock waves convergence demonstrates the possibility of significant advantage in energy expenses in comparison with the direct detonation initiation [1]. In author's findings [2], [3] the novel method for shock-to-detonation transition (SDT) due to the special channel or axisymmetrical tube walls profiling was introduced and investigated. The mechanism of initiation was determined by the gas dynamics cumulation effects when the initiating shock wave (ISW) interacted with the profiled walls. The stoichiometric propane-air mixture was considered. These results were followed by considering of essentially three-dimensional (3D) tube geometries – tube coils [4] and helical tubes [5].
The paper concerns two problems. The first one is 3D numerical investigation of SDT in stoichiometric methane-air mixture under normal conditions in a tube with parabolic contraction, connecting section of narrow diameter and conical expansion. Investigation of detonation initiation critical conditions for natural gas-air mixtures is very important and promising problem from the sense of development pulse detonation engine (PDE) [6].
The second problem is numerical study of the start-up of the small-scaled hydrogen electrochemical PDE model with the use of electrical discharge which causes the toroidal shock wave (SW) in the vicinity of detonation chamber (DC) walls. The description of main existing concepts of pulse detonation engines can be found in [6], [7]. Shock-implosion PDE concept implies the use of the imploding SW to initiate detonation in PDE DC and the parameters of the engine are discussed in [8], [9].

2. Numerical experiment methodology for the three-dimensional flows with detonation waves investigation

2.1 Mathematical model

All the calculations are performed with the use of author's original software. We use the system of equations that describe 3D unsteady flows of a reacting inviscid compressible multispecies gas mixture which in Cartesian frame of reference could be written as:

$$\frac{\partial \mathbf{q}}{\partial t}+\frac{\partial \mathbf{f}_1}{\partial x}+\frac{\partial \mathbf{f}_2}{\partial y}+\frac{\partial \mathbf{f}_3}{\partial z}=\mathbf{S},$$

$$\mathbf{q}=\begin{bmatrix}\rho_1\\ \dots\\ \rho_N\\ \rho U_x\\ \rho U_y\\ \rho U_z\\ \rho E\end{bmatrix},\ \mathbf{f}_1=\begin{bmatrix}\rho_1 U_x\\ \dots\\ \rho_N U_x\\ \rho U_x^2+p\\ \rho U_y U_x\\ \rho U_z U_x\\ (\rho E+p)U_x\end{bmatrix},\ \mathbf{f}_2=\begin{bmatrix}\rho_1 U_y\\ \dots\\ \rho_N U_y\\ \rho U_x U_y\\ \rho U_y^2+p\\ \rho U_z U_y\\ (\rho E+p)U_y\end{bmatrix},\ \mathbf{f}_3=\begin{bmatrix}\rho_1 U_z\\ \dots\\ \rho_N U_z\\ \rho U_x U_z\\ \rho U_y U_z\\ \rho U_z^2+p\\ (\rho E+p)U_z\end{bmatrix},\ \mathbf{S}=\begin{bmatrix}\omega_1\\ \dots\\ \omega_N\\ 0\\ 0\\ 0\\ 0\end{bmatrix}.$$

Here t is the time; x, y and z are Cartesian coordinates; U_x, U_y and U_z are corresponding velocity components; ρ, p and E are the density, pressure, and total specific energy of the gas mixture; ρ_k and ω_k are the density and density-variation rate due to chemical reactions of the k-th species of the mixture. The total specific energy of the gas mixture is determined by the formula:

$$E=0.5\cdot\left(U_x^2+U_y^2+U_z^2\right)+\sum_{k=1}^{N}\rho_k h_k/\rho-p/\rho,\ h_k=h_{0k}+c_{Vk}T+p_k/\rho_k,\ k=1,\dots,N,$$

where p_k, h_k, h_{0k}, c_{Vk} are partial pressure, specific enthalpy, specific enthalpy of formation and specific heat at constant volume (which is considered to be constant) of the k-th species of the mixture, N is the number of species in the mixture. Enthalpies of formation and specific heats are taken from [10].
The thermal equation of state of the mixture considered as a perfect gas is:

$$p=\sum_{k=1}^{N}p_k=\sum_{k=1}^{N}\rho_k RT/\mu_k,$$

where T is the temperature, R is the universal gas constant, μ_k is molar mass of k-th species.
For the first problem in consideration the chemical reactions are modeled by one-stage kinetics of methane combustion:

$$\mathrm{CH_4}+2\left(\mathrm{O_2}+3.762\mathrm{N_2}\right)\rightarrow\mathrm{CO_2}+2\mathrm{H_2O}+7.524\mathrm{N_2}.$$

Thus, the number of species N of the gas mixture considered is five. They are indexed in the following manner: CH_4 (k = 1), O_2 (k = 2), N_2 (k = 3), CO_2 (k = 4), H_2O (k = 5). The density-variation rate for methane is determined as:

$$\omega_1=\mu_1\psi_1,\ \psi_1=-4\cdot10^{14}\,p^{-1}\left(\rho_1/\mu_1\right)\left(\rho_2/\mu_2\right)^2\exp\left(-E^*/RT\right)\ \text{mole}/(1\cdot\text{s}),\ E^*=50\ \text{kcal/mole},$$

where ψ_1 is its molar fraction rate of variation, p is the pressure in atmospheres. The density-variation rates for the remaining species of the mixture are determined via ψ_1 and the stoichiometric coefficients in reaction as:

$$\omega_2=2\mu_2\psi_1,\ \omega_3=0,\ \omega_4=-\mu_4\psi_1,\ \omega_5=-2\mu_5\psi_1.$$

The chemical transformations in hydrogen-air mixture for the second problem are described with the detailed kinetic model which includes 17 reversible reactions [11]. The elementary reactions and constants which determine the speed of forward (subscript f in Table 1) and reverse (subscript r in Table 1) reaction

$$k=AT^b\exp\left(-E/RT\right)\ \left[\left(\text{cm}^3/\text{mole}\right)^{m-1}\cdot\text{s}^{-1}\right],$$

where m is the reaction order, are presented in Table 1.

Table 1: Parameters of detailed chemical kinetics model for hydrogen oxidation.

No.	Reaction	$\lg A_f$	b_f	E_f	$\lg A_r$	b_r	E_r
1	$H + O_2 \leftrightarrow OH + O$	14.27	0.0	16.79	13.17	0.0	0.68
2	$O + H_2 \leftrightarrow OH + H$	10.26	1.0	8.90	9.92	1.0	6.95
3	$O + H_2O \leftrightarrow OH + OH$	13.53	0.0	18.35	12.50	0.0	1.10
4	$H_2O + H \leftrightarrow OH + H_2$	13.98	0.0	20.30	13.34	0.0	5.15
5	$H_2O + M \leftrightarrow H + OH + M$	16.34	0.0	105.0	23.15	–2.0	0.0
6	$H + O_2 + M \leftrightarrow H O_2 + M$	15.22	0.0	–1.00	15.36	0.0	49.9
7	$HO_2 + O \leftrightarrow OH + O_2$	13.70	0.0	1.00	13.81	0.0	56.6
8	$HO_2 + H \leftrightarrow OH + OH$	14.40	0.0	1.90	13.08	0.0	40.1
9	$HO_2 + H \leftrightarrow H_2 + O_2$	13.40	0.0	0.70	13.74	0.0	57.8
10	$HO_2 + OH \leftrightarrow H_2O + O_2$	13.70	0.0	1.00	14.80	0.0	73.9
11	$H + O + M \leftrightarrow OH + M$	16.00	0.0	0.00	19.90	–1.0	104
12	$O_2 + M \leftrightarrow O + O + M$	15.71	0.0	115.0	15.67	–0.28	0.0
13	$H_2 + M \leftrightarrow H + H + M$	14.34	0.0	96.00	15.48	0.0	0.0
14	$H_2O_2 + OH \leftrightarrow H_2O + HO_2$	13.00	0.0	1.80	13.45	0.0	32.8
15	$H_2O_2 + O_2 \leftrightarrow HO_2 + HO_2$	13.60	0.0	42.64	13.00	0.0	1.0
16	$H_2O_2 + M \leftrightarrow OH + OH + M$	17.08	0.0	45.50	14.96	0.0	–5.1
17	$H_2O_2 + H \leftrightarrow HO_2 + H_2$	12.23	0.0	3.75	11.86	0.0	18.7

Collision efficiencies for M in:

- reaction 5: $N_2 = 1.0$, $H_2O = 20.0$;
- reaction 6: $N_2 = 1.0$, $H_2O = 21.0$, $H_2 = 3.3$;
- reaction 11: 1.0 for all the components;
- reaction 12: 1.0 for all the components;
- reaction 13: $N_2 = 1.0$, $H_2O = 6.0$, $H_2 = 3.0$, $H = 2.0$;
- reaction 16: $N_2 = 1.0$, $H_2O = 6.0$, $O_2 = 0.78$, $H_2O_2 = 6.6$.

2.2 Numerical algorithm

Method of splitting with respect to physical processes is used for the numerical solution of the problem. The system of gas-dynamic equations is discretized with respect to spatial variables by means of the finite-volume method. To enhance the accuracy the MUSCL approach [12] is used with upwind-biased third order (on uniform grids for one dimensional problems) scheme of interpolation of values at cell centers to faces [13]. The gradient of the solution vector is computed with the moving least squares method [14]. Integration over time is performed by the explicit predictor-corrector scheme with the second-order approximation. The fluxes through the computational cells faces are calculated with Godunov's method [12]. At the final stage the right-hand source terms connected with chemical reactions are taken into account by solving the corresponding system of ordinary differential equations with the use of backward differentiation formulas. The numerical algorithm is adapted for investigations to be performed on advanced multiprocessor computational systems with teraflop performance. Parallelization is performed by means of decomposition of a computational domain. For calculations we use up to 4 000 processor cores on Moscow State University supercomputer “Lomonosov”. The detailed information about the numerical procedure for the modeling of multidimensional flows with detonation waves and its parallelization can be found elsewhere [5].

2.3 Verification

The chemical kinetics model for methane oxidation was verified in [15] on the basis of the data for self-ignition delays in stoichiometric methane-air mixture obtained in the natural experiments with shock tube and the modeling of two-dimensional (2D) cellular detonation wave (DW) structure in plane channel.

The chemical kinetics model for hydrogen-air oxidation is also verified on the basis of the data for self-ignition delays in stoichiometric hydrogen-air mixture obtained in the natural experiments with shock tube [16]. Figure 1 illustrates the comparison of experimental self-ignition delays measured with different procedures with ones

calculated with the use of different kinetic mechanisms. The data from the mechanisms [17], [18] and [19] is taken from [16]. As one can see the numerical results obtained for the kinetic mechanism [11] qualitatively correspond to the experimental data; for the temperature range 1200 – 1400 K and densities important for the problems of detonation initiation and propagation – quantitatively correspond. However for the gas temperatures below 1200 K calculated ignition delays are significantly greater than experimental ones that could be connected with the reaction mechanism changing and the necessity of other reaction speed constants.

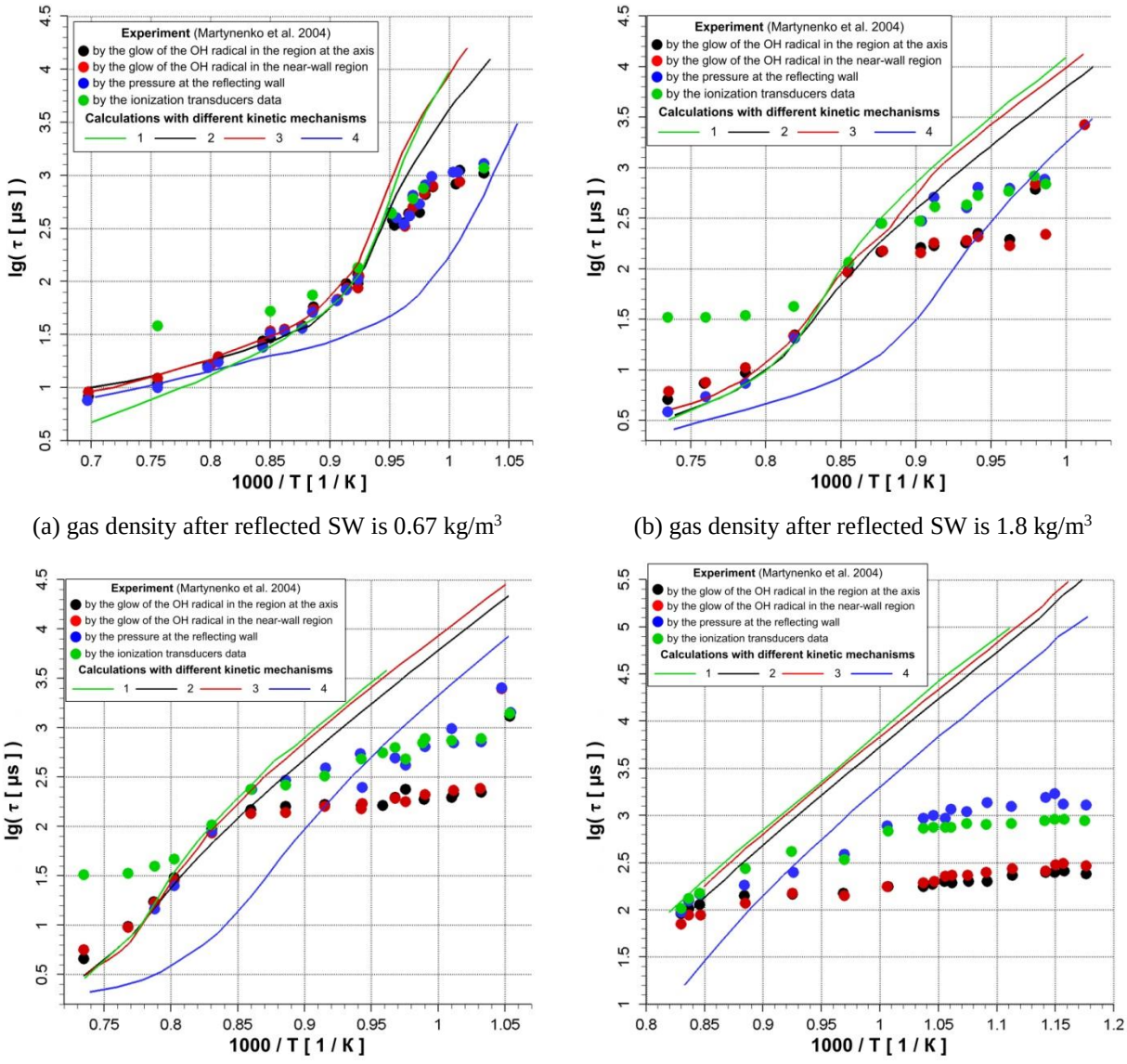

(a) gas density after reflected SW is 0.67 kg/m^3

(b) gas density after reflected SW is 1.8 kg/m^3

(c) gas density after reflected SW is 2.8 kg/m^3

(d) gas density after reflected SW is 4.32 kg/m^3

Figure 1: Comparison of calculated and experimental ignition delays in stoichiometric hydrogen-air mixture for different gas densities behind the reflected SW. 1 – Current work, reaction mechanism [11]; 2 – [17]; 3 – [18]; 4 – [19].

Another test is the modeling of cellular detonation formation in stoichiometric hydrogen-air mixture under normal conditions in a long plane channel in 2D statement. The dependency of detonation cellular structure from computational cell size is investigated with the aim to determine the most reasonable computational cell size for the further modeling of PDE chamber.

First results on numerical modeling of detonation cells in gaseous mixtures were obtained by the end of the 1970's, early 1980's, see the review and references in [20]. The mathematical models based on the fundamental conservatives laws provided the correct reproduction of the rather complicated dynamic structure of the cellular detonation front involving the leading shock, transverse waves and triple points, and the characteristic cellular pattern formed by the trajectories of triple points. At the same time a number of works appears nowadays and focuses

on the further clarification of that structures formation, for example the investigation of irregular cells in hydrogen-air mixture [21].

Consider the plane channel with the length L and the width H filled with the quiescent uniform stoichiometric hydrogen-air mixture under normal conditions. Detonation is initiated by several 'discharges' which are modeled by the areas with increased gas internal energy. All the boundaries conditions are slip walls. The formed DW evolution is the subject of the investigation. Denote the computational cell size as h, the time step as τ, computational cells total number as N_{cell}, time steps in a calculation total number – N_{steps}.

The considered test cases are characterized by the parameters presented in Table 1.

Table 2: Numerical experiments on detonation cell in hydrogen-air mixture investigation parameters.

Case No.	L, mm	H, mm	h, mm	τ, ms	N_{cell}	N_{steps}
1	500	10	$5\cdot10^{-2}$	$0.5\cdot10^{-5}$	$2\cdot10^{6}$	50 000
2	500	10	$2\cdot10^{-2}$	$0.2\cdot10^{-5}$	$12.5\cdot10^{6}$	125 000
3	500	10	$1\cdot10^{-2}$	$0.1\cdot10^{-5}$	$50\cdot10^{6}$	250 000
4	400	10	$0.5\cdot10^{-2}$	$0.5\cdot10^{-6}$	$160\cdot10^{6}$	400 000

Case 1. The numerical experiment for the most rude computational grid as is well known demonstrates the regular cellular pattern (see Figure 2). The number of detonation cells per the channel height which is formed at the distance of 0.04 m from the place of initiation remains constant and equal to 8. So the transverse detonation cell size is 1.25 mm that is too small in comparison with experimental data [22], [23].

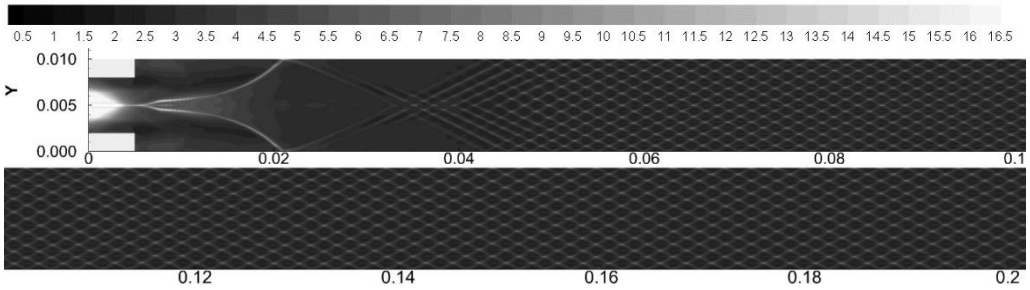

Figure 2: 'Numerical soot footprints' for the case 1. Pressure scale is in MPa, coordinates – in meters.

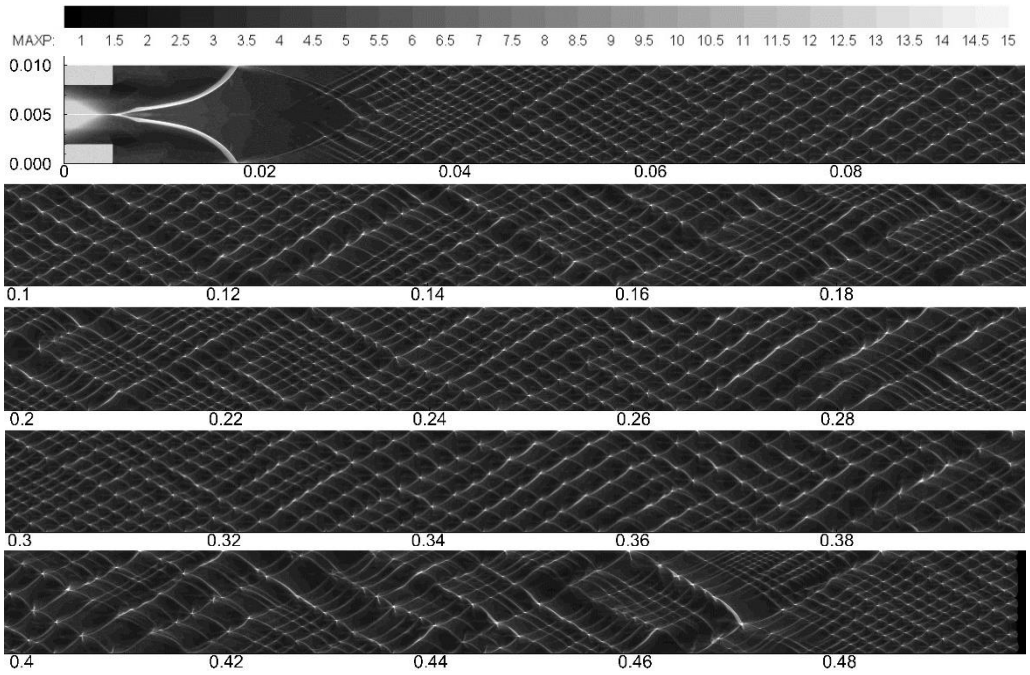

Figure 3: 'Numerical soot footprints' for the case 2. Pressure scale is in MPa, coordinates – in meters.

Case 2. The computational cell size decreasing for the channel geometry the same as in case 1 leads to the irregular cellular pattern and the averaged cross detonation cells size becomes larger (see Figure 3). The average cell size could be estimated as about 1.7 mm (6 detonation cells per the channel width) with the instant largest spatial scale of about 3 mm (see the last snapshot from 0.4 m to 0.5 mm in Figure 3).
Case 3. The further computational cell size reduction provides highly irregular detonation cells pattern (see Figure 4). Fine resolution gives the secondary cellular pattern on the primary transverse waves near the place of initiation. It is clear that thick triple points trajectories correspond to the spatial detonation cell scale of several millimeters.
The fruitful concept for irregular multilevel detonation cell structure explanation has been proposed recently in [24]. Figure 5 illustrates the detonation wave structure at some time moment. One can see that the thick triple points trajectories are formed behind the transverse detonations. The inert transverse waves give the thin tracks on the cellular pattern.

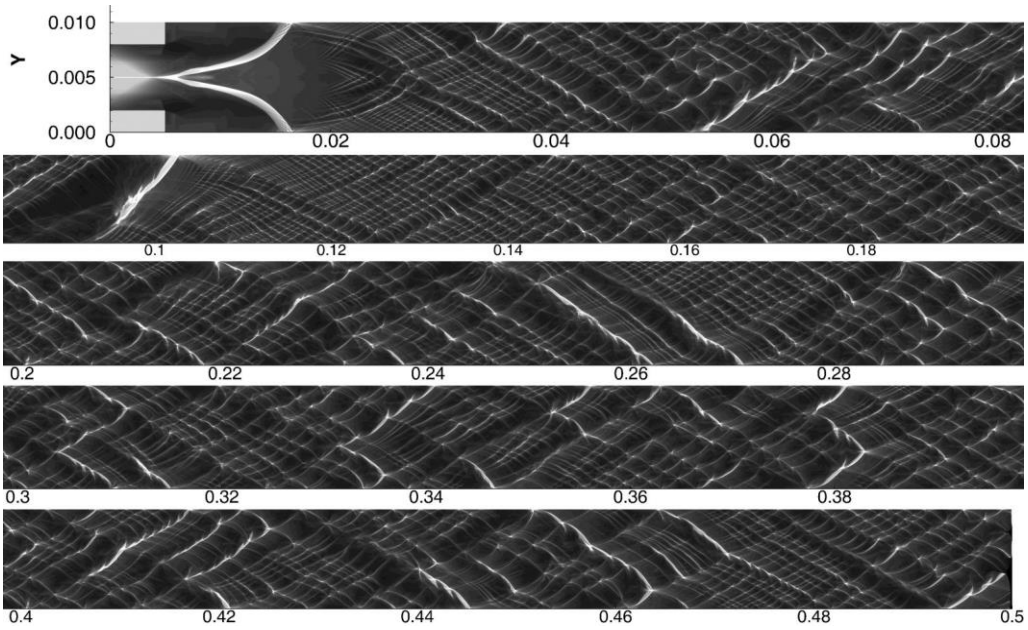

Figure 4: ‘Numerical soot footprints’ for the case 3. Pressure scale is the same as in Figure 3, coordinates – in meters.

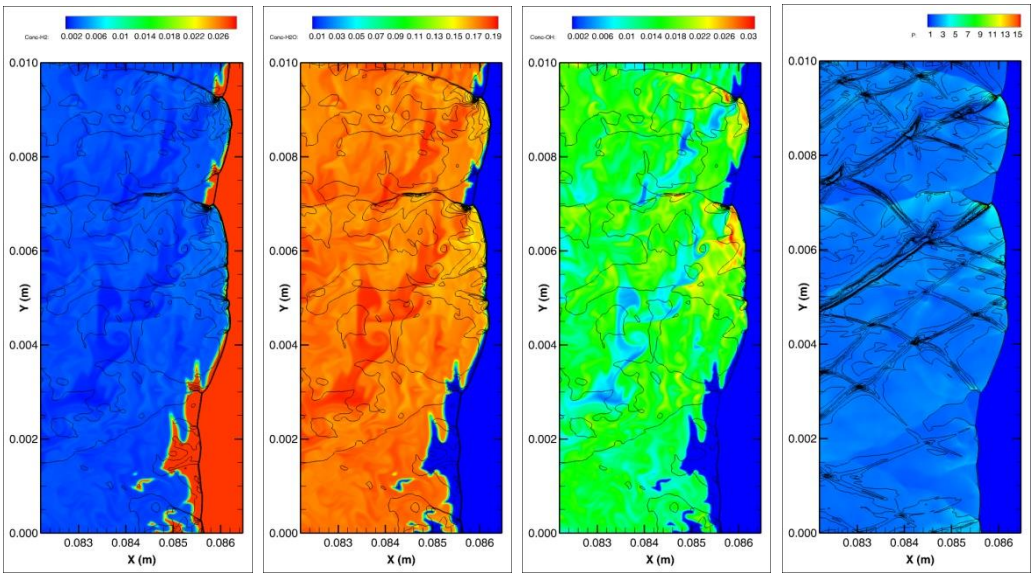

(a) (b) (c) (d)

Figure 5: Typical detonation front structure for the case 3 at some time instant: (a) H2 mass fraction field and pressure isolines, (b) H2O mass fraction field and pressure isolines, (c) OH mass fraction field and pressure isolines, (d) gas pressure field and isolines of pressure maximums.

Case 4. The cell size of the finest grid is 0.005 mm. Such resolution provides the secondary cellular structure on transverse detonations but also gives the unexpected effect. As one can see in Figure 6 detonation fails at some distance from the place of initiation. The detonation decay occurs after the formation of one strong transverse detonation wave (thick oblique tracks in the left part of the lower snapshot in Figure 6). The conclusion is made that when the grid resolution is well enough to describe zones of chemical reactions the channel geometry should satisfy the geometric limits for plane detonation propagation [25], [26]. In the considered test case the channel width is too small because the detonation cell size for stoichiometric hydrogen-air mixture is about 1.5 – 2 cm.

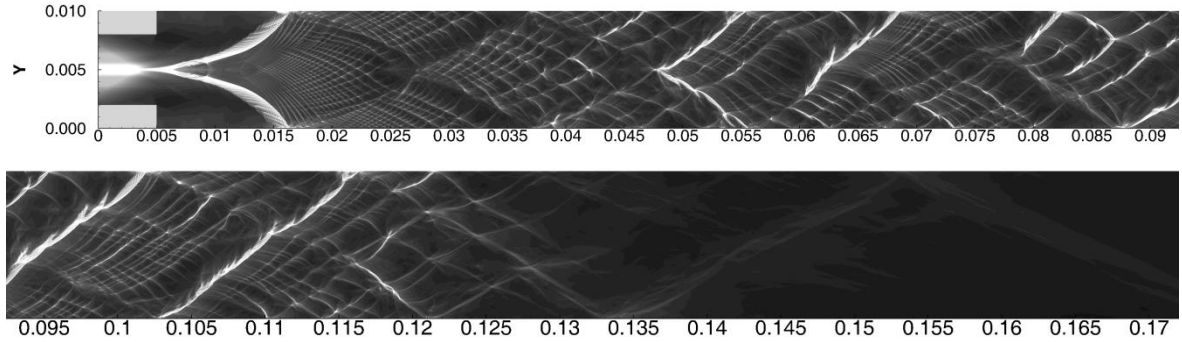

Figure 6: 'Numerical soot footprints' for the case 4. Pressure scale is the same as in Figure 3, coordinates – in meters.

3. Detonation initiation in methane-air mixture

The round tube of diameter 9.4 cm comprises five sections: Section 1 with constant cross-section, parabolic contraction (Section 2), the connecting Section 3 of constant narrow diameter, conical expansion (Section 4) and outlet Section 5 with constant cross-section (see Figure 7). Initially, the tube is filled with homogeneous, quiescent, stoichiometric methane-air mixture under normal conditions. The tube shape is determined by the geometric parameters from [15].

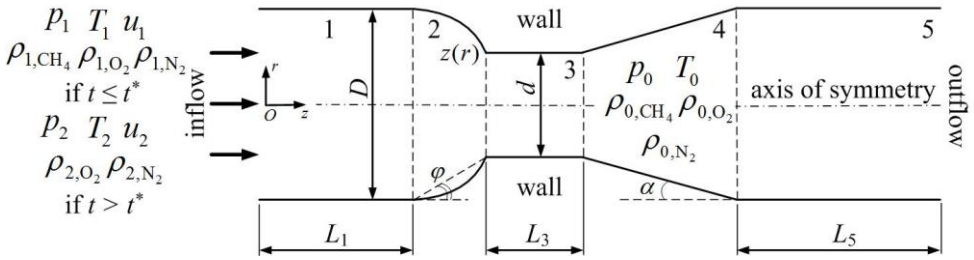

Figure 7: Scheme of the tube with profiled walls (longitudinal section).

The motion in the tube is assumed to be initiated by an ISW with zero gradients of parameters directly behind the SW front. Therefore, the boundary condition imposed on the left end of the tube from the initial time to the some time t^* is the gas inflow with the parameters of the combustible mixture corresponding to parameters behind the SW with the given Mach number. At the time t^*, the boundary condition is changed to the boundary condition for an inert gas. Other boundary conditions are slip condition on the wall and zero-gradient outflow condition on the right boundary. The calculations are performed up to the time moment when the disturbances reach the right boundary.

The shape of parabolic contraction and divergence angle of cone expansion are found which provide SDT for the ISW Mach number about 3.3. The results of 3D numerical investigation confirm in whole the results of previous 2D findings [15]. At the same time in 3D calculation the 3D detonation cellular structure is obtained which couldn't be obtained in 2D axisymmetrical study (see Figure 8). It is demonstrated the possibility of existence of regimes with the DW decaying in conical expansion.

The computational grid provided spatial resolution from 0.3 mm to 0.1 mm and included more than 100 mln. cells. Figure 9a gives an insight to the 3D pattern of the flow at the moment of local explosion formation at the symmetry axis. The part of depicted methane density isosurface of yellow color describes the blast wave location, of blue color – LSW, of red color – the retonation wave. As one can see in Figure 8 and Figure 9b in 3D case initially axial symmetric flow becomes three-dimensional after the DW spreads from the connecting Section 3 to the conical expansion because of DW front instability. Note that in 3D statement the ISW with Much number larger than 3.0 is

considered. The additional third degree of freedom in comparison with 2D statement leads to the instability growth which causes the detonation regime decay in conical expansion for the ISW Mach numbers less than 3.3.

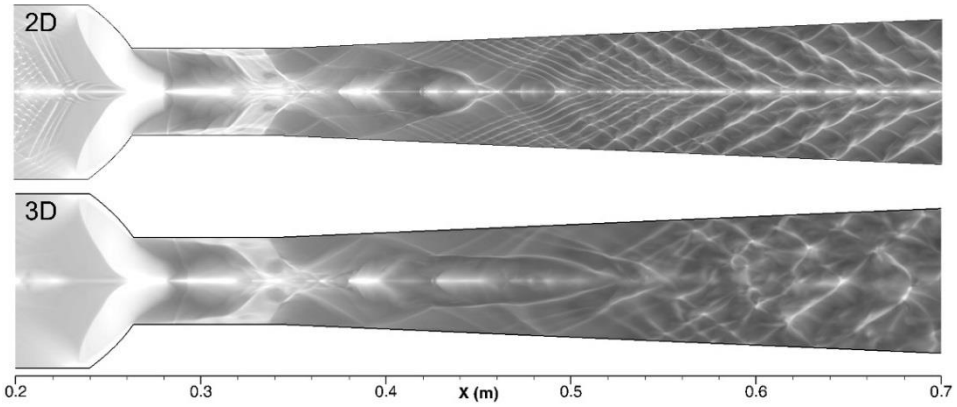

Figure 8: Comparison of 'numerical soot footprints' in 2D and 3D calculations.

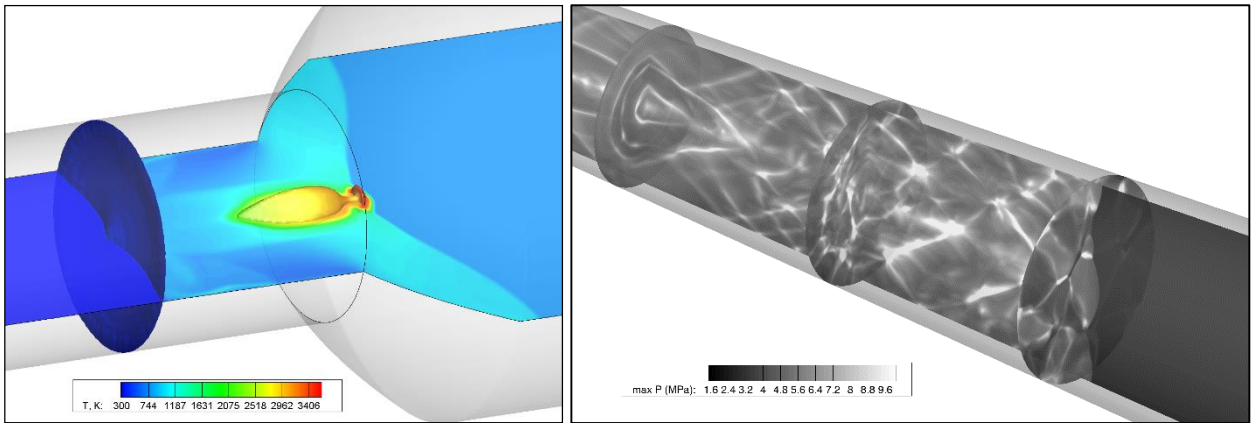

(a) (b)

Figure 9: (a) Isosurface of methane density of 0.07·10–3 g/cm^3 with the gas temperature distribution over it and predicted gas temperature in longitudinal section of the tube (in Kelvin degreases); (b) 'Numerical soot footprints' in several sectional drawings in conical expansion. DW propagation in conical expansion.

4. Detonation initiation in hydrogen-air mixture in electrochemical pulse detonation engine chamber

The hydrogen electrochemical PDE includes four major parts: inlet 1, detonation chamber 2, discharge electrodes 3, and outlet 4 (see Figure 10). In operation, the combustible mixture entering the DC is first ignited by a standard spark plug in chamber or by the contact with the residual combustion products from the previous cycle. After ignition, the turbulent flame propagates in the DC. When the turbulent flame impinges on electrodes 3 that are connected to an energy storage capacitor, the powerful electric discharge is activated. Electrodes 3 are made with a Rogowsky profile that eliminates electric field enhancement near the electrode edges. The arising 'collar', ring-type electrical discharge creates converging shock waves in the combustible mixture, leading to detonation initiation. The rest of the reactive mixture is burned in the detonation wave that travels chamber 2 [8].

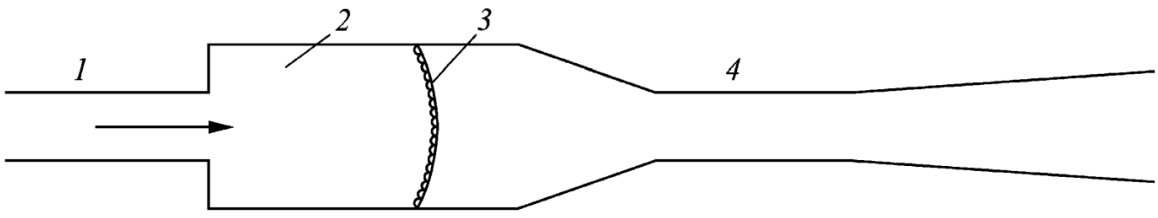

Figure 10: The scheme of electrochemical PDE.

The computational domain consists of combustion chamber only without inlet and outlet sections of the engine. The computations are performed on a grid with enough spatial resolutions about 0.015 – 0.02 mm. The total cells number is about 12.5 mln. The computations are performed in 3D statement in a sector with one cell in angular direction. The different combustion modes in chamber are investigated against electrical discharge energy – 3, 6, 7 and 10 J. At the initial time moment the computational area is filled with quiescent stoichiometric hydrogen-air mixture under normal conditions. At the distance of 15 cm from the inlet boundary near the DC wall the area with increased pressure and temperature which models the electric discharge is set. The area has a square form with 2 mm edge length in radial section. All the calculations are carried out with the constant time step equal to 2 ns.

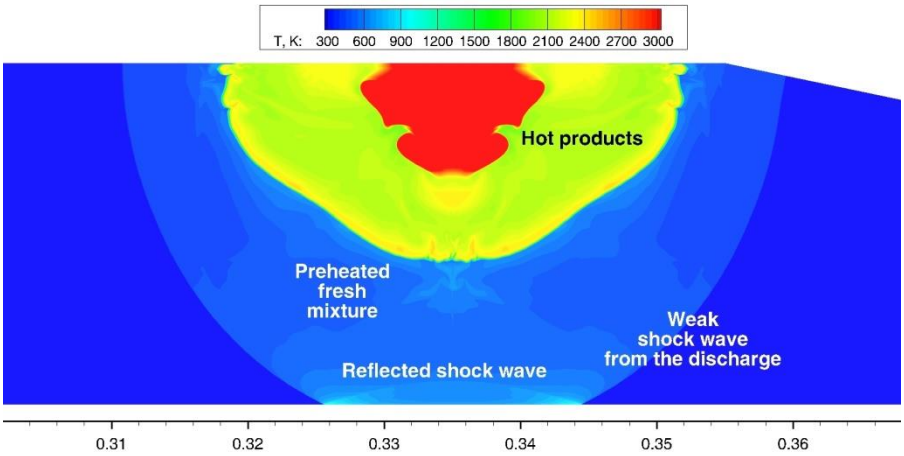

Figure 11: Predicted field of gas temperature in Kelvin degrees for the discharge energy 3 J at the time moment 21 μs. The spatial scale is in meters.

The operation cycle of the electrochemical PDE is extremely difficult because of a lot of interdependent physical and chemical processes. The aim of the current work is to investigate the initial stage of the process – detonation initiation due to the cumulation of the blast wave from the electrical discharge. Let us describe the combustion modes which occur for the different discharge energies.

It is appeared that the discharge energy 3J is not sufficient to form the strong enough SW which could due to the DC symmetry axis cumulation provide local explosion. Figure 11 makes it possible to conclude that the ISW from the discharge causes the chemical reactions behind the front just at the initial stage of the process. The insufficient ISW intensity leads to the chemical reactions decay. It is also should be noted the blast cumulation at the symmetry axis leads to the negligible temperature rise (up to about 900 K) evidently insufficient for reactive mixture self-ignition. The domain of red color in Figure 11 corresponds to the gas that initially was placed in the area of discharge.

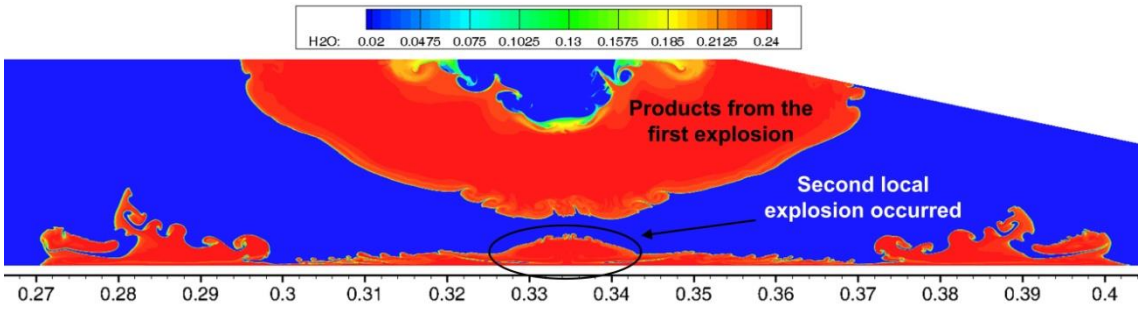

Figure 12: Predicted field of water vapor mass fraction for the discharge energy 6 J at the time moment 72 μs. The spatial scale is in meters.

For the discharge energy 6 J the blast wave cumulation provides local explosion on the DC symmetry axis in contrast to the previous case. However the strength of that explosion is not sufficient to form the DW and jets of local explosion products spread along the symmetry axis (see Figure 12).

The discharge energy 7 J gives the essentially different picture. The analysis of Figure 13 provides to reconstruct the character of the process in DC. For one thing, note the tracks of triple points directed from the place of the discharge to the symmetry axis before the moment of SW focusing.

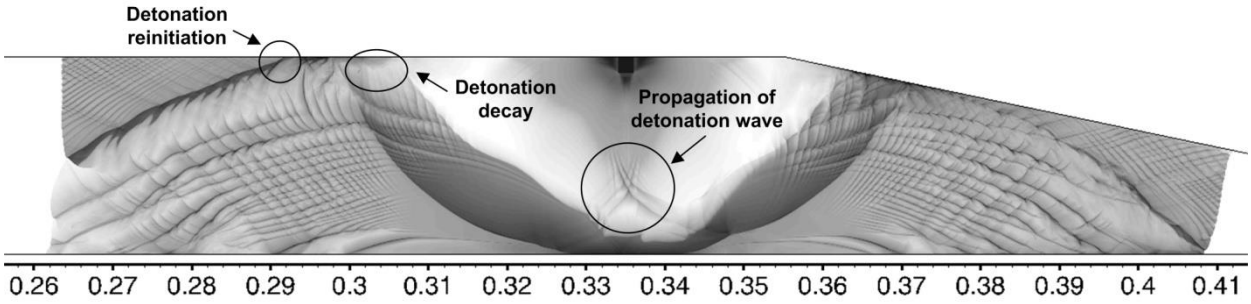

(a)

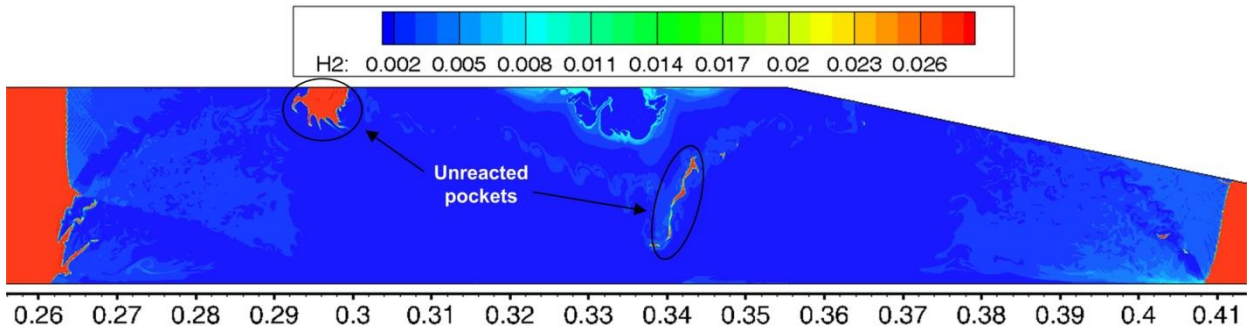

(b)

Figure 13: The process evolution for the discharge energy 7 J: (a) 'numerical soot footprints' and (b) hydrogen mass fraction at the time moment 45 μs.

Thus the discharge energy 7 J is sufficient for direct detonation initiation in DC although the DW spreads not in all directions but only in a narrow region in the direction of symmetry axis. For another thing, due to the cumulation of the SW from the discharge at the DC symmetry axis detonation waves are formed that spread to the inlet and outlet section as the 'numerical soot footprints' pattern demonstrates. The next important thing is to be noted is the 'left' DW decay (see the large unreacted pocket of fresh mixture in Figure 13b) because of geometric expansion and the following detonation reinitiation after the reflection from the wall.
In case of further increase of the discharge energy the peculiarities described above for the case of 7 J discharge energy are shown more clear. The soot footprints from the divergent DW are more distinct and vast and the detonation cell size is significantly smaller than the known experimental data because the DW is overdriven (see Figure 14).

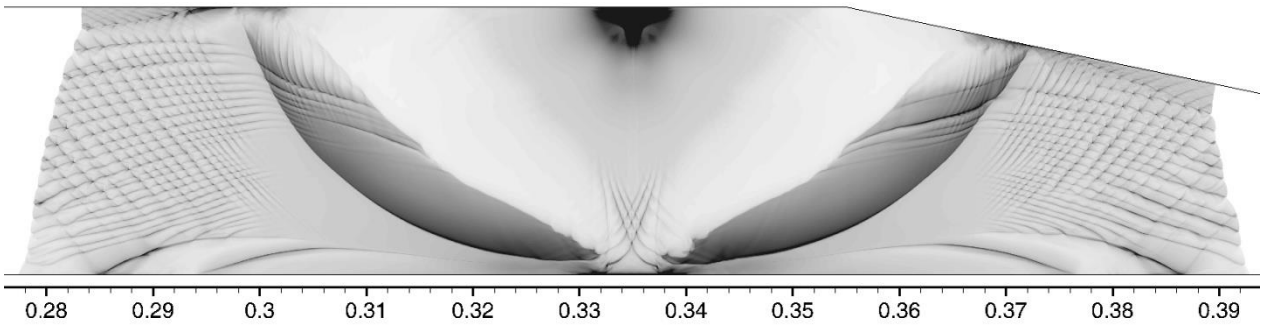

Figure 14: 'Numerical soot footprints' for the discharge energy 10 J.

5. Conclusions

In the paper the two problems concerning the detonation initiation via flow cumulation are investigated. The first one is three-dimensional numerical investigation of shock-to-detonation transition in methane-air mixture in a tube with parabolic contraction, connecting section of narrow diameter and conical expansion. The shape of parabolic contraction and divergence angle of cone expansion are found which provide shock-to-detonation transition for the initiating shock wave Mach number about 3.3. The three-dimensional structure of the formed detonation wave is

obtained. The second problem is numerical study of the start-up of the small-scaled hydrogen electrochemical pulse detonation engine model with the use of electrical discharge which causes the toroidal shock wave. Combustion modes which are realized for the different discharge energies are analyzed. It is obtained that the discharge energy 3J is too small to give local explosion at the detonation chamber symmetry axis due to the blast wave cumulation. The energy 6J provides local explosion but the detonation wave propagation fails. The energies 7 J and higher are sufficient for the engine start-up. The peculiar features of the detonation wave propagation are marked.

References

[1] Levin, V., S. Osinkin, T. Zhuravskaya, V. Markov. 2002. Determination of critical conditions for detonation initiation in a finite volume by a converging shock wave. *Comb., Expl. and Shock Waves*. 38:693–699.

[2] Frolov, S., I. Semenov, P. Komissarov, P. Utkin, and V. Markov. 2007. Reduction of the deflagration-to-detonation transition distance and time in a tube with regular shaped obstacles. *Dokl. Phys. Chem.* 415:209–213.

[3] Semenov, I., P. Utkin, V. Markov. 2009. Numerical simulation of detonation initiation in a contoured tube. *Comb., Expl. and Shock Waves*. 45:700–707.

[4] Frolov, S., I. Semenov, I. Akhmedyanov, V. Markov. 2009. Shock-to-detonation transition in tube coils. *Proc. 26th Int. Symp. Shock Waves*. V. 1. Springer Verlag. 365–370.

[5] Semenov, I., I. Akhmedyanov, A. Lebedeva, P. Utkin. 2011. Three-dimensional numerical simulation of shock and detonation waves propagation in tubes with curved walls. *Sci. Tech. Energ. Mat*. 72:116–122.

[6] Roy G., S. Frolov, A. Borisov, D. Netzer. 2004. Pulse detonation propulsion: challenges, current status, and future perspective. *Progress in Energy and Combustion Science*. 30:545–672.

[7] Wolanski P. 2011. Detonation engines. *J. KONES Powertrain and Transport*. 18:515–521.

[8] Korobeinikov, V., V. Markov, I. Semenov, S. Wojcicki. 2003. About the concept of autocyclomate energy dynamics and the modeling of electrochemical pulsating engine. *Russian J. Chen. Phys. B*. 22:73–78.

[9] Korobeinikov, V., V. Markov, I. Semenov, P. Pedrow, S. Wojcicki. 2001. Electrochemical pulse detonation engine. *High-Speed Deflagration and Detonation*. Moscow: ELEX-KM Publishers. 289–302.

[10] McBride, B., S. Gordon, M. Reno. 1993. Coefficients for Calculating Thermodynamic and Transport Properties of Individual Species. NASA Report TM-4513.

[11] Pitz, W., C. Westbrook, W. Proscia, F. Dryer. 1984. A comprehensive chemical kinetic reaction mechanism for the oxidation of n-butane. *20th Int. Symp. Comb*. 831–843.

[12] Toro, E. 1999. Riemann Solvers and numerical methods for fluid dynamics. Springer, 2nd Edition.

[13] Wesseling, P. 2001. Principles of Computational Fluid Dynamics. Springer.

[14] Gossler, A. 2001. Moving least squares: a numerical differentiation method for irregularly spaced calculation points. Sandia Report SAND2001-1669.

[15] Semenov, I., P. Utkin, I. Akhmedyanov, N. Demidov. 2012. Multidimensional modeling of detonation initiation in natural gas-air mixtures. *Proc. 9th ISHPMIE*. Cracow, Poland. Paper No. 75.

[16] Martynenko, V., O. Penyaz'kov, K. Ragotner, S. Shabunya. 2004. High-Temperature Ignition of Hydrogen and Air at High Pressures Downstream of the Reflected Shock Wave. *J. Eng. Phys. Therm*. 77:785–793.

[17] Konnov, A. 1998. Detailed Reaction Mechanism for Small Hydrocarbons Combustion. Release 0.4, http://homepages.vub.ac.be/~akonnov.

[18] Konnov, A. 2000. Development and Validation of a Detailed Reaction Mechanism for the Combustion of Small Hydrocarbons. *28th Int. Symp. Comb*. 317.

[19] Smith, P., D. Golden, M. Frenklach, N. Moriarty, B. Eiteneer, M. Goldenberg, C. Bowman, R. Hanson, S. Song, W. Gardiner, V. Lissianski, Z. Qin. GRIMECH 3.0 Reaction Mechanism. www.me.berkeley.edu/gri.mech/.

[20] Gamezo, V., D. Desbordes, E. Oran. 1999. Two-dimensional reactive flow dynamics in cellular detonation waves. *Shock Waves*. 9:11–17.

[21] Taylor, B., D. Kessler, V. Gamezo, E. Oran. 2013. Numerical simulations of hydrogen detonations with detailed chemical kinetics. *Proc. Comb. Inst.* 34:2009–2016.

[22] Bull, D., J. Elsworth, P. Shuff. 1982. Detonation Cell Structures in Fuel/Air Mixtures. *Comb. Flame*. 45:7–22.

[23] Austin, J. 2003. The role of instability in gaseous detonation. *PhD Thesis*. California Institute of Technology.

[24] Kessler, D., V. Gamezo, E. Oran. 2011. Multilevel Detonation Cell Structures in Methane-Air Mixtures. Proc. Comb. Inst. 33:2211–2218.

[25] Guirao, C., R. Knystautas, J. Lee. 1987. A Summary of Hydrogen-Air Detonation Experiments. NUREG/CR-4961, SAND87-7128, R3.

[26] Vasiliev, A. 1982. Geometric limits of gas detonation propagation. *Comb., Expl., and Shock Waves*. 18:132–136.